

Higher order extension of PDS-FEM and simulating brittle cracks

*M.L.L. Wijerathne¹, M.K. Pal², and M. Hori¹

¹Earthquake Research Institute, The University of Tokyo, Japan.

²National Research Institute for Earth Science and Disaster Resilience, Miki city, Hyogo, Japan

Presenting and corresponding author: *lalith@eri.u-tokyo.ac.jp

Abstract

Higher order extension of Particle Discretization Scheme (PDS) and its implementation in FEM framework (HO-PDS-FEM) are presented in this short paper. PDS uses the conjugate tessellation pair Voronoi and Delaunay to approximate functions and their derivatives, respectively. In HO-PDS, a function and its derivatives are approximated as the union of the local polynomial expansions. The support of the base polynomial functions being confined to the domain of each tessellation element, the PDS approximations of function and the derivatives are inherently discontinuous along the boundaries of tessellation elements. Higher order PDS-FEM utilizes these discontinuities in function approximation to model discontinuities like cracks numerically efficiently. Higher order PDS is implemented in FEM framework to solve boundary value problem of elastic solids with mode-I cracks. The verification tests show that the higher order PDS-FEM has higher accuracy and convergence rate, compared to the original 0th-order PDS-FEM [1] proposed by Hori *et al.* Several benchmark problems are presented to demonstrate the improvement in accuracy. J-integral about a mode-I crack tip field is estimated to demonstrate the improvement in accuracy of crack tip stress fields. It is shown that the singular crack tip stress field also has higher order accuracy and convergence rates, in addition to improved crack surface traction.

Keywords: Particle Discretization Scheme, higher order extension, brittle cracks, J-integral

Introduction

Real materials are far from ideal and contain numerous microscopic cracks, flaws, etc. While these have negligible effect on the ordinary deformations of materials, movements of crack tips, which are moving stress singularities, are very sensitive to these minor heterogeneities and make the crack surfaces to bend, kink and branch. Due to this high sensitivity to minor heterogeneities, even nearly identical and homogeneous samples under same loading conditions do not produce the identical crack pattern. Thus, what is required for practical applications is probability density distribution of possible crack paths, instead of theoretical crack configuration under ideal condition. Generation of probability density distribution with Monte-Carlo simulations requires efficient numerical technique to model propagating cracks.

There exists a number of numerical methods, with their own different advantages, for simulating crack propagation. Most of these methods either belong to the family of particle methods or FEM. Recent enhancements of FEM [2] enable accurate modeling of theoretically predicted crack paths. However, most FEM based methods involve significant numerical overhead (e.g. tracking crack front, especial treatment for crack branching; introducing new degrees of freedoms, etc.). Analysis of large deformation and subsequently simulating the complex cracks are easily handled in particle methods [3, 4]. Although particle methods have low computational overhead, those lacks the mathematical rigorousness. Hori *et al.* [1, 5] proposed PDS-FEM as a numerical technique which combine mathematical rigorousness of FEM and simple crack treatment of particle methods. The crack treatment of PDS is fairly simple and involves negligible numerical overhead, making it ideal for probabilistic studies of crack path variability.

The original proposal of PDS-FEM [1, 5], which we refer in this paper as 0th-order PDS-FEM, has only first order accuracy. PDS-FEM is based on Particle Discretization Scheme (PDS), which utilizes the characteristic functions of conjugate domain tessellations to approximate function and its derivatives. This paper presents an overview of higher order extension of PDS and PDS-FEM [6, 7], numerical treatments for modeling cracks and verification, and other improvements.

This short paper consists of five sections. Section two and three provide brief descriptions of higher order PDS and its implementation in FEM framework (PDS-FEM). The latter part of third section presents PDS-FEM's efficient treatment to model cracks. Some numerical results and discussions are included in the fourth section, while the fifth section presents some concluding remarks.

Higher order PDS

A unique feature of PDS is that it uses conjugate domain tessellations for approximation of functions and its derivatives. Though, any pair of tessellation could be utilized, authors have followed the former work and used Voronoi and Delaunay tessellations to approximate function and its derivatives, respectively.

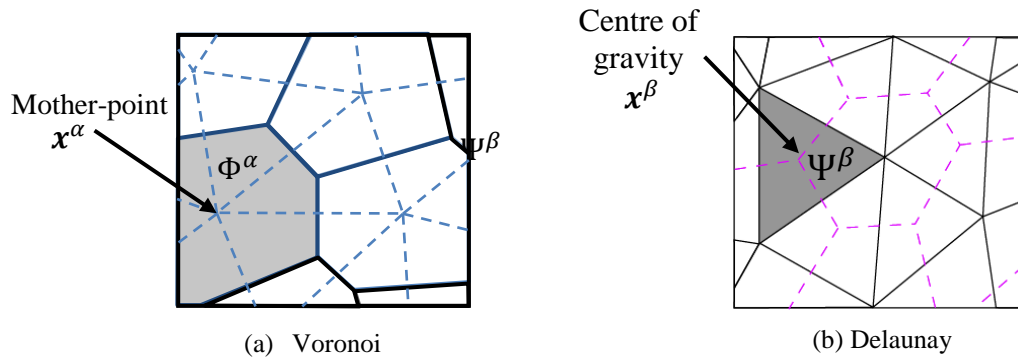


Figure 1 Voronoi and Delaunay tessellation in 2D

Assume $f(x)$ to be a target function in a given domain S ; its Voronoi and Delaunay tessellations are denoted by $\{\Phi^\alpha\}$ & $\{\Psi^\beta\}$; the set of Voronoi mother points is $\{\mathbf{x}^\alpha\}$ and the set of center of gravity of Delaunay tessellation is $\{\mathbf{x}^\beta\}$ (see Fig. 1). φ^α and ψ^β are the characteristics function of Φ^α and Ψ^β , respectively. Higher order PDS approximates $f(x)$ and its derivatives $\nabla f(x)$ as

$$f(\mathbf{x}) \approx f^d(\mathbf{x}) = \sum_{\alpha}^{N^\alpha} \sum_n^{|P^\alpha|} f^{\alpha n} P^{\alpha n} \quad (1)$$

$$\nabla f(\mathbf{x}) \approx \mathbf{g}^d(\mathbf{x}) = \sum_{\beta}^{N^\beta} \sum_n^{|Q^\beta|} \mathbf{g}^{\beta n} Q^{\beta n}$$

where $P^{\alpha n}$ and $Q^{\beta n}$ are sets of base functions. Though any suitable set of functions for modeling the problem under consideration can be used, inspired by the Taylor series we use polynomial base functions such as

$$P^{\alpha n} \in P^\alpha = \{1, (\mathbf{x} - \mathbf{x}^\alpha), \dots, (\mathbf{x} - \mathbf{x}^\alpha)^r, \dots\} \phi^\alpha(\mathbf{x}),$$

$$Q^{\beta n} \in P^\beta = \{1, (\mathbf{x} - \mathbf{x}^\beta), \dots, (\mathbf{x} - \mathbf{x}^\beta)^r, \dots\} \psi^\beta(\mathbf{x}).$$

Here, N^α and N^β are the total number of Voronoi and Delaunay tessellation elements, respectively. $|P^\alpha|$ and $|Q^\beta|$ denote the number of base functions in each of the sets.

The unknown coefficients of approximations $f^{\alpha n}$ and $g^{\beta n}$ can be found by minimizing the errors where $E^f = \int (f - f^d) ds$ and $E^g = \int (\nabla f - g^d) ds$. Minimization of these errors leads to the solving of the following linear system of equations.

$$\sum_{n=0}^{|P^\alpha|} f^{\alpha n} I^{\alpha mn} = \int f(\mathbf{x}) P^{\alpha m} ds \quad (2)$$

$$\sum_{n=0}^{|P^\alpha|} g_i^{\alpha n} I^{\beta mn} = \sum_{\alpha, l}^{N^\alpha} f^{\alpha l} \int (P^{\alpha l}(\mathbf{x}))_{,i} Q^{\beta m} ds \quad (3)$$

Here, $I^{\alpha mn} = \int P^{\alpha n} P^{\alpha m} ds$ and $I^{\beta mn} = \int Q^{\beta n} Q^{\beta m} ds$. While there is no restriction that only polynomial bases should be included in P^α and Q^β , inspired by Taylor expansion, we prefer to include polynomial bases. However, it is best to use suitable set of base functions, according to the nature of the problem.

Multiplying with the characteristic functions of each tessellation elements, the support of base functions are confined to the domain of each tessellation element. Hence the function and derivative approximations of HO-PDS have numerous discontinuities along the boundaries of respective tessellation elements.

Implementation of higher order PDS in FEM framework

The use of higher order PDS to approximate the field variables and their derivatives in FEM framework is referred as higher order PDS-FEM (HO-PDS-FEM). Consider a boundary value problem (BVP) with infinitesimal deformation of a linear elastic domain. Body forces are ignored for the sake of brevity. The standard Lagrange for linear elasticity BVP is stated as follows

$$L[\boldsymbol{\varepsilon}(\mathbf{u})] = \frac{1}{2} \int \boldsymbol{\varepsilon} : \mathbf{c} : \boldsymbol{\varepsilon} ds \quad (4)$$

Here, $\varepsilon_{ij} = \frac{1}{2}(u_{i,j} + u_{j,i})$ is the strain tensor and \mathbf{c} is fourth order elasticity tensor defining linear stress-strain relation. Setting the first variation $\delta L = 0$, we can obtain the strong form of the governing equations and essential boundary conditions.

Following the HO-PDS the unknown displacement \mathbf{u} is approximated as

$$u_i(\mathbf{x}) \approx u_i^d(\mathbf{x}) = \sum_{\alpha}^{N^\alpha} \sum_n^{|P^\alpha|} u_i^{\alpha n} P^{\alpha n}. \quad (5)$$

Further, following the definition of derivative approximation of HO-PDS, the derivatives of displacement are approximated as $u_{i,j} \approx \sum_{\beta, m} u_{ij}^{\beta m} Q^{\beta m}$. Based on Eq. 2, $u_{ij}^{\beta m}$ can be expressed as

$$u_{ij}^{\beta m}(\mathbf{x}) = \sum_{m'}^{|Q^\beta|} w^{\beta mm'} \sum_{\alpha}^{N^\alpha} \sum_n^{|P^\alpha|} u_i^{\alpha n} \int_{\Psi^\beta} Q^{\beta m'} (P^{\alpha n})_{,j} ds$$

$$= \sum_{m'}^{|Q^\beta|} w^{\beta mm'} \sum_{\alpha}^{N^\alpha} \sum_n^{|P^\alpha|} u_i^{\alpha n} h_j^{\beta \alpha m' n} \quad (6)$$

where $[w^{\beta mn}]^{-1} = [I^{\beta mn}] = [\int_{\Psi^\beta} Q^{\beta n} Q^{\beta m} dv]$. Now the strain field can be approximated as

$$\varepsilon_{ij}(\mathbf{x}) \approx \sum_{\beta}^{N^\beta} \sum_n^{|Q^\beta|} \varepsilon_{ij}^{\beta n} Q^{\beta n},$$

where $\varepsilon_{ij}^{\beta n}$ can be expressed using Eq. 6 as

$$\varepsilon_{ij}^{\beta n} = \sum_{m'}^{|Q^\beta|} w^{\beta mm'} \sum_{\alpha}^{N^\alpha} \sum_n^{|P^\alpha|} \frac{1}{2} (h_j^{\beta \alpha m' n} u_i^{\alpha n} + h_i^{\beta \alpha m' n} u_j^{\alpha n}). \quad (7)$$

For the sake of brevity, let's express Eq. 7 in tensor form as

$$\boldsymbol{\varepsilon}^{\beta m} = \text{symm}(\mathbf{B}^{\beta m \alpha n} \otimes \mathbf{u}^{\alpha n}), \quad (8)$$

where $B_i^{\beta m \alpha n} = \sum_{m'}^{|Q^\beta|} w^{\beta mm'} h_i^{\beta \alpha m' n}$.

Similarly stress tensor $\boldsymbol{\sigma}$ can be approximated as $\sigma_{ij}(\mathbf{x}) \approx \sum_{\beta}^{N^\beta} \sum_n^{|Q^\beta|} \sigma_{ij}^{\beta n} Q^{\beta n}$. The elasticity tensor \mathbf{c} is also approximated using the characteristic functions of Delaunay tessellation as $c_{ijkl}(\mathbf{x}) \approx \sum_{\beta}^{N^\beta} c_{ijkl}^{\beta} \psi^{\beta}(\mathbf{x})$. It is straight forward to obtain $\sigma_{ij}^{\beta n} = c_{ijkl}^{\beta} \varepsilon_{kl}^{\beta n}$.

Substituting the Eq. 8 into L in Eq. 4 and setting its first variation to zero (i.e. $\delta L = 0$), the following governing matrix equation of HO-PDS-FEM can be obtained.

$$\sum_{\alpha', n, n', m'} w^{\beta n n'} \cdot (\mathbf{B}^{\beta n \alpha m} \cdot \mathbf{c}^{\beta} \cdot \mathbf{B}^{\beta n \alpha' m'}) \cdot \mathbf{u}^{\alpha' m'} = \mathbf{0} \quad (9)$$

According to the above equation, the element stiffness matrix of HO-PDS-FEM is

$$\mathbf{K}^{\beta} = \mathbf{w}^{\beta} \cdot \mathbf{B}^{\beta n \alpha m} \cdot \mathbf{c}^{\beta} \cdot \mathbf{B}^{\beta n \alpha' m'} \quad (10)$$

Size of this element stiffness matrix depends on the space dimensions and number of basis functions used in analyzing the target problem. For example, the size is $(6 \times |P^\alpha|) \times (6 \times |P^\alpha|)$ for a 2D Delaunay triangle, and $(12 \times |P^\alpha|) \times (12 \times |P^\alpha|)$ for 3D Delaunay tetrahedral.

Modeling brittle crack in HO-PDS-FEM

Major advantage of PDS-FEM is its simple and efficient treatment for modeling propagating discontinuities like cracks. The displacement field approximation $u_i^d(\mathbf{x})$ is inherent with discontinuities along each boundary of Voronoi elements Φ^α , $\partial\Phi^\alpha$, as a consequence of

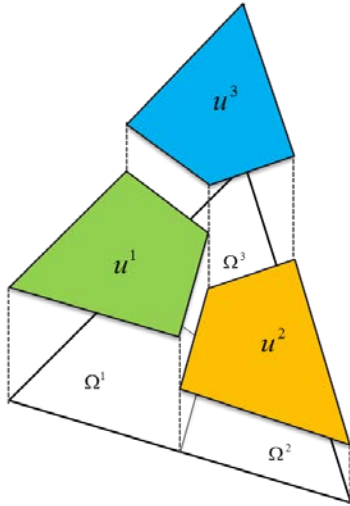
limiting the support of each polynomial base $P^{\alpha n}$ to the domain of the corresponding tessellation element Φ^α . Figure 2(a) shows an exaggerated illustration of a displacement component approximated with PDS over a Delaunay tessellation. As explained in this subsection, HO-PDS-FEM utilizes these existing discontinuities along $\partial\Phi^\alpha$'s to numerically efficiently model moving discontinuities in BVPs.

The contribution to the strain from the above mentioned discontinuities can be isolated by expressing base functions with compact support within each Voronoi as $P^{\alpha n} = F^{\alpha n}(\mathbf{x}) \phi^\alpha(\mathbf{x})$ and substituting to $h_j^{\beta\alpha m' n}$ in Eq. 6.

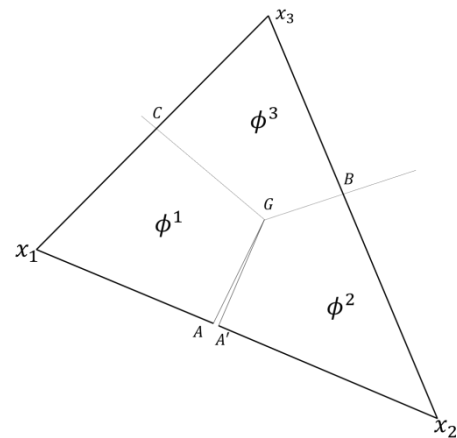
$$\begin{aligned}
h_j^{\beta\alpha m' n} &= \int_{\Psi^\beta} Q^{\beta m'} (P^{\alpha n})_{,j} ds \\
&= \int_{\Psi^\beta} Q^{\beta m'} \left((F^{\alpha n})_{,j} \phi^\alpha + F^{\alpha n} \phi_{,j}^\alpha \right) ds \\
&= \int_{\Psi^\beta} Q^{\beta m'} (F^{\alpha n})_{,j} \phi^\alpha ds + \int_{\partial\Phi^\alpha} Q^{\beta m'} F^{\alpha n} n_j dl
\end{aligned} \tag{11}$$

In the above equation, the surface integration $\int_{\partial\Phi^\alpha} Q^{\beta m'} F^{\alpha n} n_j dl$ carries the contribution to strain ε_{ij} from the above mentioned discontinuities along boundaries $\partial\Phi^\alpha$; note that we have used the Gauss divergence theorem. Eliminating this contribution is equivalent to introducing a discontinuity to the physical problem by removing the contribution from an infinitesimally thin neighborhood along $\partial\Phi^\alpha$.

As an example, an opening crack AGA' as shown in Fig. 2(b), along the common boundary of Voronoi elements Φ^1 and Φ^2 in Fig. 2(a), can be modelled by simply dropping the contributions $\int_{AG} Q^{\beta m'} F^{\alpha n} n_j dl$ and $\int_{GA'} Q^{\beta m'} F^{\alpha n} n_j dl$ while evaluating element stiffness matrix \mathbf{K}^β of the Delaunay element encompassing the crack surface.



(a) Discontinuities in the approximated displacement field obtained with PDS-FEM



(b) Mode-I crack AGA' is modeled by dropping contribution from a thin neighborhood of boundary between Φ^1 and Φ^2 .

Figure 2. Modeling a mode-I crack

Most of the existing numerical tools require introduction of additional nodes, enrichment functions, etc., subsequently adding substantial numerical overhead and/or complex process. On the other hand, higher order PDS-FEM only requires only re-calculation of an element stiffness matrix eliminating the contributions $\int_{\partial\Phi^\alpha} Q^{\beta m'} F^{\alpha n} n_j dl$ along the required Voronoi boundaries $\partial\Phi^\alpha$. This very low numerical overhead in modeling cracks is a notable feature which makes PDS-FEM one of the most numerically efficient numerical treatment for modeling cracks. This is especially useful in simulation of 3D crack propagation in large scale models.

Numerical examples

As explained above, a function or vector field approximated with PDS consists of numerous discontinuities along each Voronoi boundary. The use of such discontinuous approximations in solving BVP is rare and one may doubt about the quality of the solution. In this section some numerical examples are presented to demonstrate that PDS-FEM is accurate and higher order versions have the expected higher accuracy and convergence rates. A major advantage of PDS-FEM being the numerical efficient crack treatment, majority of the examples given in this sections are to demonstrate the accuracy stationary crack modelled with HO-PDS-FEM.

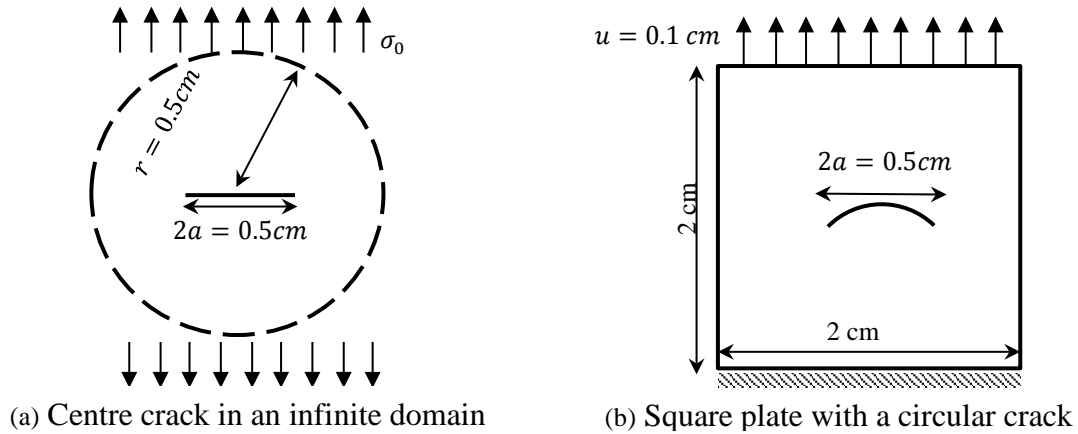


Figure 3 Considered numerical examples with stationary model-I cracks

Problem setting

A classical mode-I finite crack in an infinite domain (see Fig. 3(a)) is chosen as a numerical example to verify crack tip singularity modelled with HO-PDS-FEM. An arch shape crack shown in Fig. 3(b) is analyzed to demonstrate that it can model nearly traction free crack surfaces. For all the problems provided in this section, Young's modulus of 1GPa and Poisson's ratio of 0.33 are assumed.

Results with two different pairs of base functions sets are compared to demonstrate the improvement in accuracy. The first case is with lowest order base functions $P^\alpha = \{1\}$ and $Q^\beta = \{1\}$, which is referred as 0th-order PDS-FEM. The other case is with the polynomial bases $P^\alpha = \{1, (x - x^\alpha), (y - y^\alpha)\}$ and $Q^\beta = \{1, (x - x^\beta), (y - y^\beta), (x - x^\beta)^2, (y - y^\beta)^2, (x - x^\beta)(y - y^\beta)\}$, which is referred as 1st-order PDS-FEM.

Results and discussion

Figure 4 shows the stress component along the right half of the crack surface. As seen, in the neighborhood of crack tip, HO-PDS-FEM's solution has a large deviation from the analytical

solution. However, σ_{yy} is in good agreement with analytic solution elsewhere. Moreover, higher order PDS-FEM reproduces the traction free crack-surface, which is a significant improvement compared to 0th-order PDS-FEM. Analytical solution of this boundary value problem is of nature of $\sqrt{r}\text{Sin}(\theta/2)$ and cannot be accurately approximated as a linear combination of polynomials. Hence, this significant disagreement in the crack tip neighborhood is not unexpected.

The best way to eliminate this large deviation in the crack tip neighborhood is to utilize the analytic solution for crack tip stress field as the basis functions of higher order PDS-FEM. Another less precise technique is to adjust the point of inflection of polynomial bases in Q^β only for the Delaunay elements encompassing crack tips. It is found that choosing the mid-point of Delaunay edge, through which crack enters (see Fig. 5), as the point of inflection of polynomial bases in Q^β improves crack tip stress field.

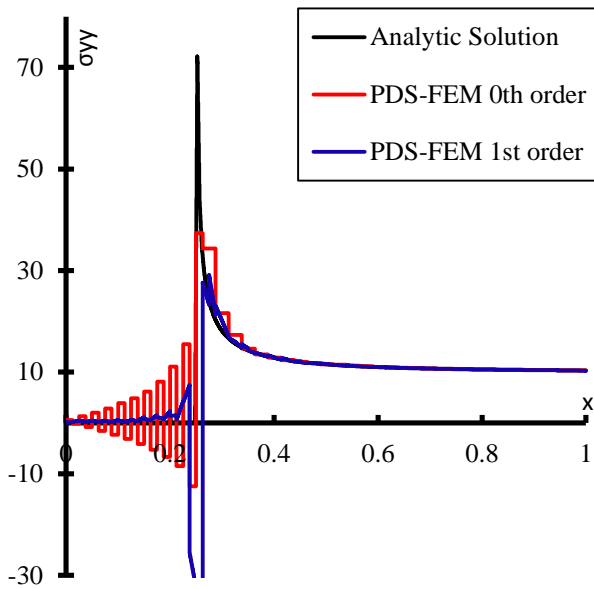


Figure 4 σ_{yy} along the right half of crack line

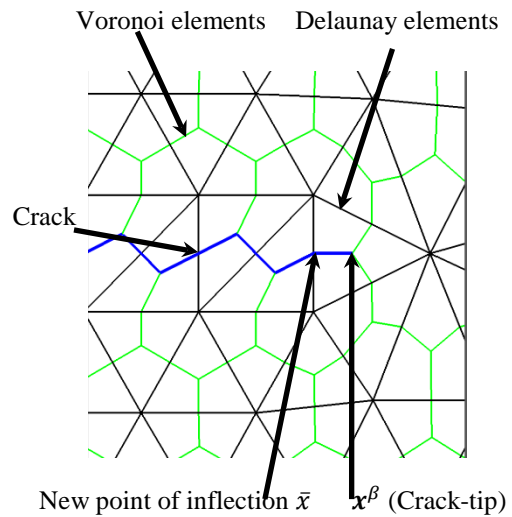


Figure 5 Point of inflection

Figure 6 compares the results of 0th-order and 1st-order PDS-FEM with analytic solution, when point of inflection is moved to the entry point of the crack. As is seen, the results are in good agreements with the analytic solution. Also, the crack surface remains nearly traction free, which is noteworthy improvement compared to 0th-order (see Fig. 6). Further, Fig. 7 shows the J-integral with different number of degrees of freedoms. As is seen, both the accuracy and rate of convergence have improved with 1st-order PDS-FEM.

Although the accuracy of crack tip stress field can be improved using analytical solutions of crack tip stress field, the above presented less precise approach by moving the point of inflexion is attractive in large scale simulations since it does not increase the numerical overhead. Though the use of analytic solution of crack tip stress field as the basis functions improves the accuracy, it increases the numerical overhead, leading to load imbalance in parallel computing and lower scalability. On the contrary, moving of point of inflexion does not involve any additional numerical overhead.

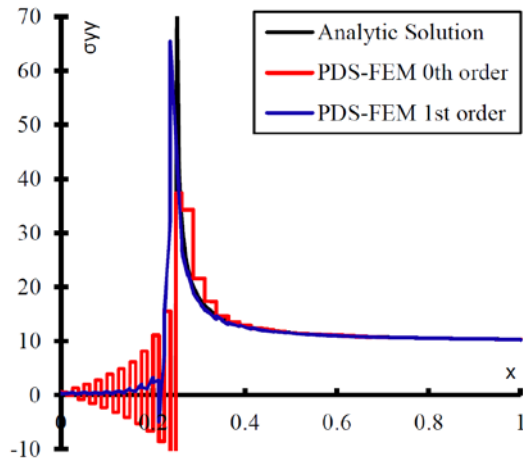


Figure 6 σ_{yy} along the right half of crack

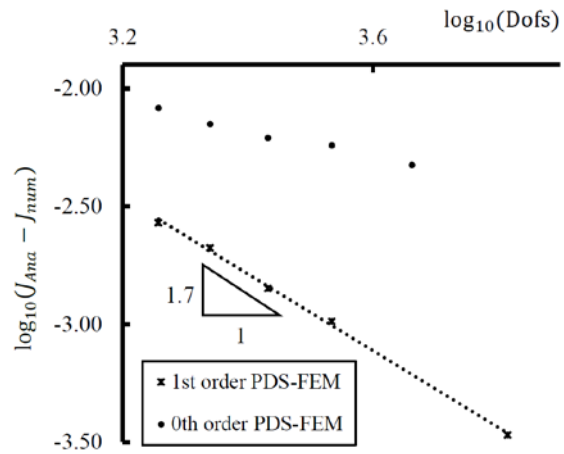
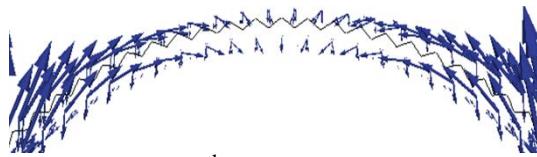
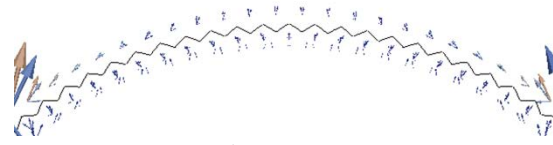


Figure 7 Convergence rate of J-integral

Figure 8 compares the tractions, obtained with 0th-order and 1st-order PDS-FEM, along the curved crack surfaces in the rectangular plate. It can be clearly seen that the 1st-order PDS-FEM can reproduce nearly traction free crack surfaces, and it is a significant improvement compares to 0th-order.



(a) 0th-order PDS-FEM



(b) 1st-order PDS-FEM

Figure 8 Traction normal to crack surfaces

Unlike most other FEM based crack treatments, PDS-FEM does not emphasizes modeling the crack tip and crack surface precisely. Instead PDS-FEM tries model crack tip and surface to a sufficient degree of accuracy for practical problems focusing on lower numerical overhead so that large scale 3D crack propagation problems can be solved efficiently. However, as shown above the crack tip and surfaces modeled with HO-PDS-FEM have a fairly high accuracy and convergence rates. The crack surfaces modeled with PDS-FEM.

Uniformly pressured thick hollow cylinder

A thick cylinder subjected to internal and external pressure is considered to verify the 3D implementation of HO-PDS-FEM. Figure 8 illustrates the problem settings. The boundary conditions over the top and bottom surfaces are set to reproduce plain strain conditions. In this 3D problem, the set of polynomial bases used are $P^\alpha = \{1, (x - x^\alpha), (y - y^\alpha), (z - z^\alpha)\}$ and $Q^\beta = \{1, (x - x^\beta), (y - y^\beta), (x - x^\beta)^2, (y - y^\beta)^2, (z - z^\beta)^2, (x - x^\beta)(y - y^\beta), (x - x^\beta)(z - z^\beta), (y - y^\beta)(z - z^\beta)\}$.

Figure 10 compares the analytic solutions and numerical results of radial displacement u_r and strain component ϵ_{rr} along a radial line. A quick comparison advocates the improvement in solution with the mesh refinement, and that the numerical solutions are in good agreement with analytic solution. For this specific setting, u_r reaches its maximum at $r = 0.2$. Figure 11 shows

the error of u_r at $r = 0.2$ for several tessellations with different element sizes. As is seen, the error diminishes at second order rate with respect to the number of degrees of freedoms, which is the expected.

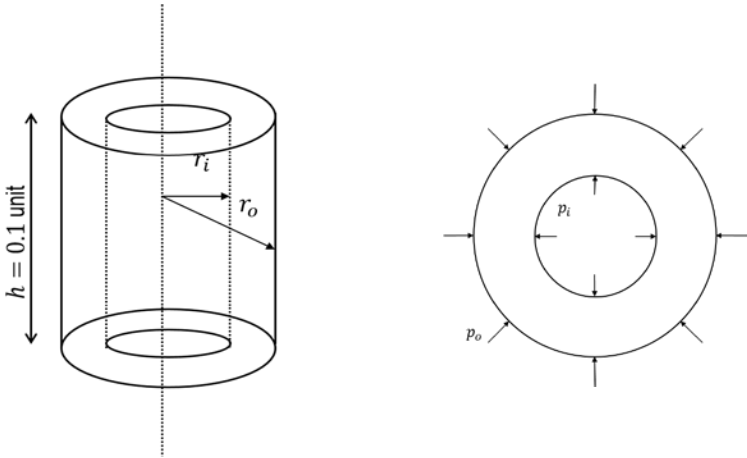


Figure 9 Thick hollow cylinder applied with uniform internal and external pressure

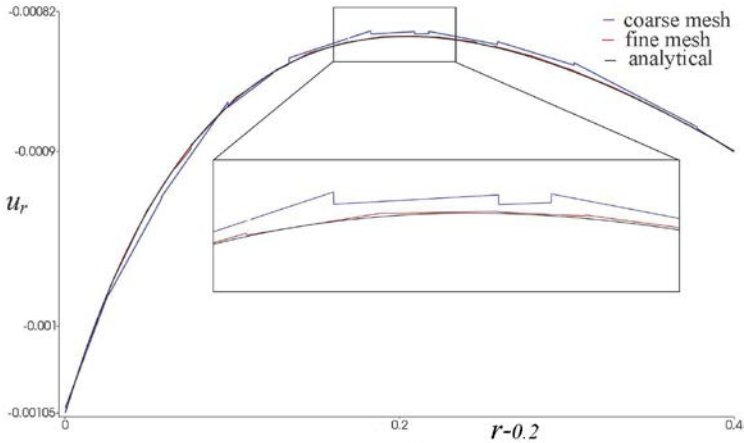


Figure 10 Comparison of displacement along radial direction u_r

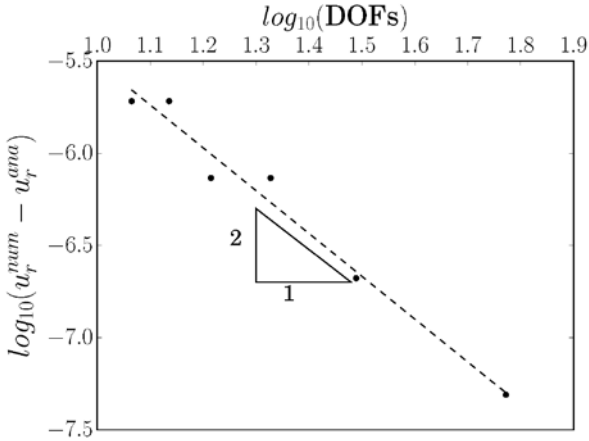


Figure 11 Convergence rate of the displacement along radial direction

Concluding remarks

Implementation of higher order PDS-FEM and its application to simulated brittle stationary cracks are presented. With numerical example, it is demonstrated that HO-PDS-FEM provides higher accuracy and theoretically expected convergence rates. Two major advantages of HO-PDS-FEM over former 0th-order PDS-FEM are the improvement in the accuracy of crack tip stress field and significant reduction in traction along the model-I crack surfaces. Like in the former 0th-order implementation, the numerical treatment for modeling cracks with HO-PDS-FEM also numerically efficient to simulate crack propagation in large scale 3D models.

References

- [1] Hori, M., Oguni, K., Sakaguchi, H., (2005) Proposal of FEM implemented with particle discretization scheme for analysis of failure phenomena, *J. of Mech. and Phys. of Solids*, **53** 681–703.
- [2] Moes, N., Dolbow, J., Belytschko, T., (1999) A finite element method for crack growth without remeshing. *International Journal for Numerical Methods in Engineering*, **46**(1) 131-150.
- [3] Gingold, R.A., Monaghan, J.J., (1977) Smoothed particle hydrodynamics: theory and application to non-spherical stars. *Monthly Notices of the Royal Astronomical Society*, **181** 375–389.
- [4] Schlangen E., Garboczi E.J., (1997) Fracture simulations of concrete using lattice models: computational aspects. *Engrg. Frac. Mechanics*, **57**(2) 319–332.
- [5] Wijerathne, M.L.L. , Oguni, K., Hori, M. (2009) Numerical analysis of growing crack problem using particle discretization scheme, *Int. J. for Numerical Methods in Engineering*, **80** 46-73.
- [6] Pal, M.K., Wijerathne, L., Hori, M., Ichimura, T., Tanaka, S. (2014) Implementation of Finite Element Method with higher order Particle Discretization Scheme, *J. of Japan Society of Civil Engineers, Ser.A2* **70**(2) 297-305.
- [7] Pal, M.K., Wijerathne, L, Hori, M., Ichimura, T. (2015), Simulation of cracks in linear elastic solids using higher order Particle Discretization Scheme-FEM, *J. of Japan Society of Civil Engineers, Ser.A2* **71**(2) 327-337